HHS Public Access

Author manuscript

Sci Transl Med. Author manuscript; available in PMC 2023 July 04.

Published in final edited form as:

Sci Transl Med. 2022 August 31; 14(660): eabj7465. doi:10.1126/scitranslmed.abj7465.

A targetable pathway in neutrophils mitigates both arterial and venous thrombosis

Lalitha Nayak[1,*,†], **David R. Sweet**[2,3,4,†], **Asha Thomas**[1], **Stephanie D. Lapping**[2,3], **Kenneth Kalikasingh**[1], **Annmarie Madera**[2,3], **Vinesh Vinayachandran**[2,3], **Roshan Padmanabhan**[2,3], **Neelakantan T. Vasudevan**[2,3], **Jay T. Myers**[5], **Alex Y. Huang**[5], **Alvin Schmaier**[1], **Nigel Mackman**[6], **Xudong Liao**[2], **Andrei Maiseyeu**[2,7], **Mukesh K. Jain**[8]

[1]Division of Hematology and Oncology, University Hospitals Cleveland Medical Center, Cleveland, OH 44106, USA.

[2]Case Cardiovascular Research Institute, Case Western Reserve University, Cleveland, OH 44106, USA.

[3]Harrington Heart and Vascular Institute, University Hospitals Cleveland Medical Center, Cleveland, OH 44106, USA.

[4]Department of Pathology, Case Western Reserve University, Cleveland, OH 44106, USA.

[5]Department of Pediatrics, Case Western Reserve University, Cleveland, OH 44106, USA.

[6]Division of Hematology, University of North Carolina, Chapel Hill, NC 27599, USA.

[7]Department of Biomedical Engineering, Case Western Reserve University, Cleveland, OH 44106, USA.

[8]Warren Alpert Medical School of Brown University, Providence, R1 02903.

Abstract

Arterial and venous thrombosis constitutes a major source of morbidity and mortality worldwide. Long considered as distinct entities, accumulating evidence indicates that arterial and venous thrombosis can occur in the same populations, suggesting that common mechanisms are likely operative. Although hyperactivation of the immune system is a common forerunner to the genesis of thrombotic events in both vascular systems, the key molecular control points remain poorly

*Corresponding author. lxn64@case.edu.
†These authors contributed equally to this work as co-first authors.

Author contributions: L.N., D.R.S., A. Maiseyeu, and M.K.J. conceived the project and designed the experiments. L.N., D.R.S., A.T., S.D.L., K.K., A. Madera, V.V., N.T.V., X.L., and A. Maiseyeu performed animal and cell-based experiments. V.V. performed sequencing experiments. V.V., R.P., and D.R.S. analyzed sequencing data. J.T.M. and A.Y.H. performed two-photon microscopy experiments. A.S. and N.M. provided guidance for thrombosis experiments. L.N., D.R.S., A.T., and A. Maiseyeu contributed to data visualization and figure generation. L.N. and D.R.S. drafted the original manuscript. All authors discussed the results and commented on the manuscript.

Competing interests: The authors declare that they have no competing interests.

Data and materials availability: All data associated with this study are present in the paper or the Supplementary Materials. RNA sequencing data have been deposited into Gene Expression Omnibus (GEO, www.ncbi.nlm.nih.gov/geo/) under accession number GSE208336.

SUPPLEMENTARY MATERIALS
www.science.org/doi/10.1126/scitranslmed.abj7465

understood. Consequently, antithrombotic therapies targeting the immune system for therapeutics gain are lacking. Here, we show that neutrophils are key effectors of both arterial and venous thrombosis and can be targeted through immunoregulatory nanoparticles. Using antiphospholipid antibody syndrome (APS) as a model for arterial and venous thrombosis, we identified the transcription factor Krüppel-like factor 2 (KLF2) as a key regulator of neutrophil activation. Upon activation through genetic loss of KLF2 or administration of antiphospholipid antibodies, neutrophils clustered P-selectin glycoprotein ligand 1 (PSGL-1) by cortical actin remodeling, thereby increasing adhesion potential at sites of thrombosis. Targeting clustered PSGL-1 using nanoparticles attenuated neutrophil-mediated thrombosis in APS and KLF2 knockout models, illustrating the importance and feasibility of targeting activated neutrophils to prevent pathological thrombosis. Together, our results demonstrate a role for activated neutrophils in both arterial and venous thrombosis and identify key molecular events that serve as potential targets for therapeutics against diverse causes of immunothrombosis.

One-sentence summary:

Activated neutrophil migration and adhesion can be targeted in arteriovenous thrombotic disorders such as antiphospholipid antibody syndrome.

Editor’s Summary:

Thwarting thrombosis

Arterial and venous thrombosis can affect nearly every organ system and likely share common drivers. Thus, identifying those common drivers may reveal a therapeutic target to prevent disease caused by thrombosis. Here, Nayak *et al.* used antiphospholipid antibody syndrome (APS) as a model to identify neutrophils as a driver of immunothrombosis. Neutrophil-specific deletion of Krüppel-like factor 2, a transcription factor regulating neutrophil activation, worsened disease in mice by driving neutrophil activation. In contrast, targeting of P-selectin glycoprotein ligand 1 (PSGL-1) on activated neutrophils attenuated APS symptoms in mice by preventing downstream adhesion and thrombosis development. Together, the authors show that neutrophils, and, more specifically, PSGL-1, may be useful clinical targets for APS and other causes of immunothrombosis.

INTRODUCTION

Thrombotic disease affecting arterial and venous circulation affects nearly every organ system and makes up a major source of morbidity and mortality worldwide. It has long been understood that mechanisms of thrombosis differed between arterial and venous vessels, in part due to vastly different hemodynamic and metabolic stresses that they experience (1, 2). Under certain conditions, however, individuals experience both arterial and venous thrombosis, suggesting shared mechanisms of disease. Antiphospholipid antibody syndrome (APS) is one such disorder, uniquely characterized by devastating arterial and venous thrombosis in young individuals, leading to myocardial infarction, ischemic stroke, recurrent pregnancy loss, and multiorgan failure. The mainstay of therapy for chronic thrombotic conditions such as APS is long-term anticoagulation, an approach that is only modestly effective, as recurrent thrombotic events still occur and treatment is associated with an

increased risk for bleeding. Thus, a better understanding of the molecular and cellular determinants of arterial and venous thrombosis is crucial to the development of safer therapeutic alternatives.

Classically, studies of thrombosis have focused largely on the endothelium, platelets, and coagulation factors. However, studies over the past decade have underscored the importance of inflammation in the thrombotic process, termed immunothrombosis, and have led to the appreciation that myeloid cells participate in arterial and venous thrombotic events (3, 4). Collectively, the emerging role of innate immune cells not only constitutes a paradigm shift in our understanding of fundamental mechanisms controlling thrombosis but also offers new opportunities for antithrombotic therapies targeting myeloid cells. Here, we identified neutrophils as operant in both arterial and venous thrombosis and developed therapeutics targeting activation cascades stemming from the loss of a central transcription factor, Krüppel-like factor 2 (KLF2).

RESULTS

Neutrophils are critical players in arterial thrombosis

Because of their capacity to monitor the intact vasculature, neutrophils are able to play an important role in regulating venous thrombosis (5). In arterial thrombosis, however, the role of neutrophils is less clear, despite their presence in murine and human arterial thrombi. To determine whether neutrophils may serve as a cellular link in arterial and venous thrombosis, we used a model of APS whereby mice were injected with purified antiphospholipid antibodies (aPLs) from patients with APS. Mice injected with aPL developed arterial thrombi significantly ($P < 0.001$) faster than immunoglobulin G (IgG) control in a model of carotid artery injury (Fig. 1A). Upon antibody-mediated depletion of neutrophils, however, this effect was greatly attenuated (Fig. 1B). In mice that had not been treated with aPL, induction of neutropenia had no effect on thrombus formation, indicating that the presence of nascent neutrophils is not required for thrombosis (fig. S1A). Conversely, infusion of neutrophils harvested from aPL-injected mice into untreated recipients worsened arterial thrombosis (Fig. 1C). Together, these data suggest that neutrophils are both necessary and sufficient to worsen immunothrombosis in an APS model, highlighting a previously underappreciated role for these cells in arterial thrombosis.

Loss of neutrophil-expressed KLF2 worsens arterial and venous thrombosis

The transcription factor KLF2 has previously been identified as a dominant tonic repressor of myeloid cell activation under acute and chronic inflammatory conditions (6, 7). Furthermore, global loss of KLF2 augments experimental thrombosis (8). To determine whether decreased KLF2 expression is operative in aPL-mediated thrombosis, we harvested neutrophils from aPL-treated mice as well as from patients with APS and observed profound reductions in *KLF2* transcript (Fig. 1, D and E). Treatment of a myeloid cell line directly with aPL also reduced the expression of *Klf2*, suggesting a direct effect from antibody administration (fig. S1B). Given the activation phenotype of myeloid cells deficient in KLF2, we hypothesized that loss of myeloid KLF2 may worsen thrombosis, thus providing a potential molecular switch governing aPL-mediated thrombosis. To explore this, we

subjected mice with myeloid-specific deletion of KLF2 [LysM$^{cre/cre}$KLF2$^{fl/fl}$, K2KO (KLF2 knockout)] and controls (LysM$^{cre/cre}$, LysM) to arterial and venous thrombosis models (fig. S1C). There were neither appreciable differences in cell counts, coagulation parameters, and platelet reactivity nor neutrophil size between genotypes (fig. S1, D to H). K2KO mice exhibited both shortened times to arterial thrombosis (Fig. 2A) and heavier clot weights in the inferior vena cava (IVC) ligation model of venous thrombosis (Fig. 2B). This effect appeared to be dependent on K2KO neutrophils as neutrophil depletion rescued arterial and venous thrombotic phenotypes, whereas monocyte and macrophage depletion with clodronate liposomes did not (Fig. 2, C to E, and fig. S1, I and J). Similar to studies in aPL-treated mice (Fig. 1C), transfusion of K2KO neutrophils into LysM mice was sufficient to worsen arterial and venous thrombotic burden (Fig. 2, F to H). Neutrophilia or neutropenia alone did not affect thrombosis in LysM mice, demonstrating that resting neutrophils do not substantially contribute to thrombosis.

KLF2 deletion unleashes the prothrombotic functions of neutrophils

Neutrophils contribute to thrombosis through numerous mechanisms, including neutrophil extracellular trap (NET) release and production of prothrombotic tissue factor (TF) (5). To determine whether loss of KLF2 catalyzes these functions in arterial and venous thrombosis, we first explored whether K2KO neutrophils are more prone to NETosis. After stimulation with *N*-formyl-Met-Leu-Phe (*f*MLP), K2KO neutrophils released more NETs in vitro, a phenomenon recapitulated in vivo in IVC clots after ligation (Fig. 3, A and B). Although numerous components are needed for proper NET formation, neutrophil elastase (NE) and myeloperoxidase (MPO) are essential in chromatin decondensation and for decorating NETs for bactericidal functions (9). Whereas other components remained unaffected, K2KO neutrophils expressed higher NE and MPO, likely contributing to increased NET release (Fig. 3C and fig. S2A). Functionally, this translated to higher thrombotic potential, as administration of a selective inhibitor of MPO negated the prothrombotic milieu established by K2KO neutrophils (Fig. 3D).

Recent studies identify neutrophil TF as important in arterial thrombus generation (10). We thus hypothesized that increased neutrophil TF activity is likely contributing to the shortened time to arterial thrombosis noted with KLF2 deletion. Consistent with our hypothesis, bone marrow neutrophils isolated from K2KO mice show increased TF expression and activity as compared to controls (Fig. 3E and fig. S2, B and C); further, preincubation of K2KO neutrophils with TF-neutralizing antibody (1H1) increased time to thrombosis (Fig. 3F). Incubation of LysM neutrophils with 1H1 before infusion did not increase time to thrombosis, further demonstrating that quiescent neutrophils do not contribute to thrombosis through TF and showing that neutrophil activation is key in neutrophil TF–mediated thrombosis exacerbation (fig. S2D).

To determine whether KLF2 reduces transcriptional activity of the TF promoter in response to inflammation, we overexpressed KLF2 in the context of p65 overexpression or lipopolysaccharide (LPS) treatment. As predicted, KLF2 overexpression abrogated TF promoter activity in response to inflammatory activation, suggesting that KLF2 attenuates nuclear factor κB–induced transcription of this target (fig. S2E). *KLF2* mutations in zinc

finger domains have previously been identified in human lymphoid malignancies (11). To determine whether these naturally occurring mutations affect KLF2's ability to regulate TF, we repeated the promoter assays and found that mutant KLF2 failed to reduce p65-induced TF promoter activity, suggesting a potential DNA binding inhibitory function of KLF2 in TF transcription (fig. S2F). Whether these or similar mutations occur in prothrombotic patient populations remains to be explored. Collectively, these data show that KLF2 transcriptionally regulates neutrophil TF and that loss of KLF2 leads to heightened TF activity, worsening arterial thrombosis.

K2KO neutrophils are transcriptionally primed for migration and adhesion

Next, we sought to explore how loss of KLF2 in neutrophils affected transcriptional networks important in the pathogenesis of thrombosis. RNA sequencing of peripheral blood neutrophils from LysM and K2KO mice demonstrated more than 2000 differentially expressed genes (DEGs) enriched in processes such as immune cell activation, adhesion and migration, actin remodeling, and metabolism (Fig. 4, A and B). The extent of differential expression represented KLF2-regulated transcription, rather than a genome-wide sequencing artifact (fig. S3, A and B). Comparing transcriptional profiles of K2KO neutrophils to neutrophils from patients with APS (12) revealed similar signatures. Among enriched Kyoto Encyclopedia of Genes and Genomes (KEGG) and Gene Ontology (GO) processes by either group, 50 to 64% were shared with the other group, with shared gene sets including immune cell activation, adhesion, and actin cytoskeleton remodeling processes (Fig. 4C). These transcriptional signatures had functional effects on migration in K2KO neutrophils, as demonstrated by in vitro transwell migration and in vivo peritoneal recruitment assays (Fig. 4, D and E). This mechanism appeared to be operative in arterial and venous thrombosis as well. Clots were evaluated early in thrombus formation (4 hours for venous and 10 min for arterial) to investigate kinetics of neutrophil migration between experimental groups; these data demonstrated that K2KO mice have substantially higher neutrophil counts at arterial and venous vessel walls early in thrombus formation (Fig. 4, F and G). Wild-type mice challenged with aPL also had higher neutrophil counts along the endothelium early in the carotid artery thrombotic process, demonstrating similarities between the APS and K2KO models (Fig. 4H). This phenomenon was recapitulated in LysM/K2KO mice using intravital microscopy visualization of labeled leukocytes and platelets in a microvascular thrombosis model of the ear. Within minutes of thermal injury, K2KO leukocytes were more quickly recruited to the site of thrombosis, with platelet accumulation shortly following (fig. S4, A to C). Leukocyte accumulation was noted to increase at 1 to 1.5 min after injury in LysM and K2KO mice, although absolute numbers per injured area were higher in K2KO mice. Platelet accumulation followed and was noted to increase at about 3 min. Together, these data demonstrate that loss of KLF2 conferred enhanced migratory capacity in neutrophils, likely contributing to worsened clot burden in arterial and venous thrombosis. This mechanism is potentially important in immunothrombotic states such as APS, as demonstrated by similar transcriptional signatures between human and murine models of disease.

Cortical actin remodeling was observed in KLF2-deficient murine neutrophils and in neutrophils from individuals with APS

Neutrophil migration and adhesion are highly dependent on precise spatial coordination of cell surface ligands to maximize contact with adhesion receptors on endothelial cells. This occurs through cytoskeletal remodeling below the cell membrane, promoting clustering of adhesion molecules on membranous structures such as microvilli, lamellipodia, pseudopodia, and uropods (13-15). Because APS and K2KO neutrophils demonstrate transcriptional enrichment of actin remodeling processes and their downstream functional consequences (such as increased motility and adhesion), we hypothesized that loss of KLF2 permitted actin remodeling to occur, thereby promoting cortical actin accumulation and the formation of membranous protrusions. Staining of F-actin in unstimulated neutrophils revealed a thickening of cortical actin in K2KO neutrophils with noticeable projections in the form of microvilli and pseudopods (Fig. 5, A and B). Quantification of cortical actin demonstrated that increases in integrated density in K2KO neutrophils were due to increased area and not fluorescent intensity, suggesting that reorganization of F-actin, versus expression, is responsible for the increased cortical actin content (Fig. 5C and fig. S4D). Further, neutrophils from patients with APS exhibit similar reorganization of cortical actin (Fig. 5D).

PSGL-1–mediated neutrophil adhesion promoted arterial and venous thrombosis

Although KLF2-regulated actin dynamics presented a function of this transcription factor in neutrophil biology, the downstream consequences of this in the context of aPL-mediated thrombosis were unclear. To determine whether loss of KLF2 results in increased rolling and adhesion in an adhesion molecule–specific manner, we used a dynamic in vitro system in which LysM and K2KO neutrophils were added to microfluidic flow chambers coated with various adhesion molecules. Whereas K2KO neutro4phils did not demonstrate enhanced adhesion or rolling along channels coated with classical adhesion molecules, vascular cell adhesion protein 1 (VCAM-1), and intercellular adhesion molecule 1 (ICAM-1) (fig. S5, A and B), P-selectin–coated chambers exhibited significant differences in rolling and adhesion between K2KO and LysM cells ($P < 0.01$; Fig. 6A). K2KO neutrophils traversed through P-selectin–coated chambers far slower and demonstrated increased rolling behavior and also attached to the channel at substantially higher numbers. This effect was ameliorated by precoating K2KO neutrophils with anti–PSGL-1 (P-selectin glycoprotein ligand 1)–neutralizing antibody, demonstrating that a substantial component of the K2KO adhesion effect is due to PSGL-1/P-selectin interactions (Fig. 6B and fig. S5C). Blockade of PSGL-1–P-selectin interactions on K2KO neutrophils before infusion rescued the thrombotic phenotype in vivo, underscoring the importance of enhanced adhesion as a purveyor of immunothrombosis (Fig. 6, C to E).

Nanoparticle targeting of clustered PSGL-1 protects against arterial and venous thrombosis

Studies from the past decade have elucidated mechanisms by which many adhesion molecules are shuttled and clustered along the cell membrane in distinct units that increase the strength of interaction with cognate binding partners. PSGL-1, for instance,

is redistributed onto uropods upon neutrophil activation (16-18). Because surface receptor redistribution is largely dependent on the very cytoskeletal remodeling processes that are enriched in K2KO and APS neutrophils, we hypothesized that PSGL-1 would redistribute onto uropods, thereby reducing rolling velocity and increasing adhesion. Despite exhibiting no differences in expression of PSGL-1 (fig. S6, A and B), K2KO neutrophils exhibit increased uropod formation as well as redistributing and clustering PSGL-1 on these polarized membrane structures (Fig. 6, F and G). Proper PSGL-1 adhesive function is largely dependent on posttranslational modifications to its extracellular domains including N- and O-linked glycosylation (19). Further, glycosylation of PSGL-1 appears to be critical in its role in affecting thrombosis (20). Loss of KLF2 was also associated with modest transcriptional changes in glycosylation machinery important in the processing of PSGL-1 function, providing additional potential mechanistic linkage between KLF2 and PSGL-1 function (fig. S3B).

Targeting PSGL-1 as an anti-inflammatory therapeutic has been proposed in numerous diseases, including aPL-induced thrombosis (12, 21, 22). Given the widespread expression pattern of PSGL-1 across numerous cell types, along with limitations in effectively dosing infused antibodies to a sufficient local concentration (the need for high-infusion doses to achieve a sufficient concentration seen by circulating cells), we hypothesized that targeting anti–PSGL-1 monoclonal antibodies (mAbs) to clustered PSGL-1 would increase both cell type specificity and local concentration to activated neutrophils. To accomplish this, we used a nanoparticle (NP)–based delivery system by which model polystyrene latex NPs were decorated with anti–PSGL-1 immunoglobulin, yielding high-surface area-to-volume concentration of the mAbs, thus mimicking “clustering” in a manner similar to its target PSGL-1 clustering on uropods (fig. S6C). We previously reported a highly efficient template-based hybrid NP synthesis method that allows for precise control of surface modification while allowing for NP size to be dictated by a chosen template, such as polystyrene latex (23).

We hypothesized that maintaining a constant concentration of anti–PSGL-1 on varying particle sizes (from 0.02 to 2 μm) would allow for discrimination of activated versus resting neutrophils and versus other cell surface–expressing PSGL-1. A typical batch of NPs yielded anti–PSGL-1– or IgG-coated NPs in a desired size distribution depending on the template (fig. S6D). Of the five sizes tested, the smallest, 0.02-μm (20 nm)–diameter templated NPs were the most effectively targeted to activated (K2KO), but not resting (LysM), neutrophils as seen by fluorescence microplate assays (fig. S6E). Conversely, control IgG–decorated NPs did not demonstrate an activation-biased targeting (fig. S6F). Anti–PSGL-1–coated NPs (anti–PSGL-1 NP) were active in functional assays in vitro and blocked K2KO, but not LysM, neutrophils from their attachment to a P-selectin–coated surface (Fig. 7A). Although anti–PSGL-1 mAb alone inhibited activated cell adhesion in these assays, anti–PSGL-1 NP improved this effect, reducing cell adhesion by 50%. In vivo, antibody-coated NPs were biocompatible, endogenously cleared, and did not induce appreciable differences in neutrophil clustering (fig. S6, G and H).

Intravenous injection of anti–PSGL-1 NPs overcame the K2KO prothrombotic state, effectively returning values to those of wild-type mice in thrombosis and decreasing

neutrophil adhesion along the vessel wall (Fig. 7, B to D, and fig. S6I). The beneficial effect of anti–PSGL-1 NPs appeared to be specific to activated neutrophils, as incubation of K2KO neutrophils with anti–PSGL-1 NPs before infusion protected against arterial and venous thrombosis to a similar extent as injection of NPs into the circulation, whereas incubating LysM neutrophils with anti–PSGL-1 NPs did not affect thrombosis (Fig. 7, E to G, and fig. S6J).

The efficacy of anti–PSGL-1 NPs to inhibit arterial and venous thrombosis in the K2KO model suggests potential use in attenuating aPL-driven thrombosis. To this end, we administered anti–PSGL-1 NPs to mice injected with aPL and demonstrated that blockade of clustered anti–PSGL-1 attenuated thrombosis in the arterial and venous systems, establishing this approach as a viable option for intervention of thrombosis (Fig. 7, H to J). NP delivery of anti–PSGL-1 antibodies reduced the antibody concentration needed. At concentrations $^{1}/_{25}$ of the experimental dose, anti–PSGL-1 NPs maintain their therapeutic effect, whereas anti–PSGL-1 antibody alone lost efficacy against carotid artery thrombosis (Fig. 7K). Last, unlike aggressive anticoagulation that represents the mainstay treatments for arterial and venous thrombosis, intravenous treatment with PSGL-1 targeting agents did not increase bleeding risk (fig. S6K).

DISCUSSION

Reactive immune cells and the release of inflammatory mediators in response to tissue injury are now well-described additions to the classical factors underlying thrombosis that were first described by Virchow. Despite this, therapeutic strategies against thrombosis have focused downstream of these interactions and have largely ignored the role of immune cells. Here, we explored the neutrophil as a central mediator of both arterial and venous thrombosis. Our findings identify transcriptional and biophysical mechanisms by which neutrophils participate in thrombosis through augmented actin remodeling and adhesion, NETosis, and TF release through down-regulation of KLF2. Further, these data establish NP-mediated neutrophil inhibition as an improved targeting strategy in arterial and venous thrombosis (fig. S7).

Uncovering which transcription factors sit at the center of pathological systems opens up a web of interconnected processes that each provide a potentially targetable axis for therapeutic intervention. Although the neutrophil has recently been identified to be a central cellular effector of arterial and venous thrombosis, we have now identified that loss of KLF2 appears to be a key inciting event that transforms a quiescent neutrophil, unlikely to contribute to thrombosis, to one that is primed for migration, adhesion, and the release of prothrombotic factors. Given that neutrophil KLF2 concentrations are diminished in patients with APS-related thrombosis, it is of great interest to determine whether the extent of KLF2 depression is related to severity of disease. Although the cohort used in this study were heterogeneous with regard to disease severity and comorbid conditions, previous work has identified inverse correlations between KLF2 expression and severity of inflammatory conditions (24), potentially indicating a role for neutrophil KLF2 expression as a biomarker for thrombotic potential. Larger patient populations will be needed to investigate the utility of KLF2 in predicting thrombotic events in APS and in other prothrombotic states,

such as cancer-induced thrombosis and coronavirus disease 2019 (COVID-19)–associated thrombosis.

Precisely how this factor is down-regulated in response to inflammatory cues also remains to be explored. Current work is underway to identify the signaling cascade that occurs when neutrophils are exposed to aPL and how KLF2 may serve as a key responder to these circulating antibodies. aPL isolated from patients with APS consists of many antibody species (such as lupus anticoagulant, anticardiolipin, and anti–β_2 glycoprotein 1) that may work through convergent or divergent mechanisms in diminishing KLF2 (25). Anti–beta-2 glycoprotein 1, for example, is capable of signaling through Toll-like receptor 4, a known upstream axis to KLF2 reduction (26-29). Regardless, identifying pathways upstream and downstream of KLF2 will illuminate additional therapeutic targets limiting aberrant neutrophil activation in prothrombotic states.

Because of their abundance and sentinel nature, neutrophils are especially amenable to NP-based therapies and have been extensively studied as carriers of drug-laden NPs to sites of inflammation (30, 31). Here, we propose that neutrophils can be targets of NP-based therapies in addition to effectors. Because actin cytoskeleton remodeling creates membranous protrusions which allow neutrophils and other amoeboid leukocytes to increase surface area against vessel walls and concentrate adhesion proteins into clusters, we reasoned that this phenomenon could be leveraged in designing therapeutics that more specifically and efficiently target activated neutrophils. Preclinical models using PSGL-1–neutralizing antibodies as anti-inflammatory agents have been explored in numerous diseases, including ischemia and reperfusion injury, Crohn's disease, and malignancies [reviewed in (21)]. Recent work from Knight *et al.* (12) suggests a similar approach for aPL-mediated thrombosis. Given the widespread expression pattern of PSGL-1 on endothelial cells, monocytes, platelets, and lymphocytes, systemic administration of high-dose anti–PSGL-1 antibody would broadly coat the hemo-vascular system with little specificity (32-35). By concentrating anti–PSGL-1 on low-diameter NPs, we created cognate structures to uropods and pseudopods on the surface of neutrophils. Through this, we believe that NP delivery provides improved spatial distribution of targeting antibodies, thereby increasing local concentrations at neutrophil cell surfaces. This is analogous to the ability of CD4 antibody-rich NPs to more effectively neutralize HIV than soluble neutralizing agents (36). Last, although this work was performed in the context of APS-related thrombosis, we believe that it has implications for many disease states characterized by arterial and venous thrombosis including cancer, infections (such as that seen in the COVID-19 pandemic), and other autoimmune disorders.

One limitation of these studies is inherent in reducing complex processes such as thrombosis into simplified models; although this work underscores the contributions of neutrophils as predominant cells in arterial and venous thrombosis, in reality, there are numerous intercellular interactions that are critical for the formation of thrombi. Hence, the molecular mechanisms whereby aPL triggers pathologic clotting likely involve endothelial cells, platelets, and other circulating leukocytes (37-39). Additional work investigating the interplay between neutrophils and other effectors of thrombosis will be critical in better characterizing cellular networks central to arteriovenous thrombosis. Another confounding

factor for this work is the well-described heterogeneity of autoantibodies that cause thrombosis in APS. Although we demonstrate a role for aPL isolated from patients with APS in decreasing KLF2 and causing thrombosis in a neutrophil-dependent fashion, the specific antibody species contributing to each of these processes remains to be explored. Delineating axes of activation and mechanisms of disease, therefore, are clouded using nonspecific stimuli. Ongoing experiments attempting to isolate specific antibody species (anti–beta-2 glycoprotein 1, antiprothrombin, anticardiolipin, and others) from patients are underway to address mechanistic specificity. Last, establishing a murine model of acute thrombosis secondary to chronic inflammatory disease creates a unique set of challenges with regards to translatability to human disease. The chronicity of APS results in patients' cells experiencing a continuous onslaught from autoantibodies, whereas murine models rely on multiple individual doses of antibodies. The transcriptional and functional consequences of this can be appreciated in cell models of immune cell priming and tolerance (40). In these systems, repetitive stimulation of myeloid cells can result in differing responses based on when the cells were last stimulated. Whether such a phenomenon occurs in aPL-induced thrombosis remains to be explored.

Although the feasibility of long-term NP-based therapeutics in humans remains debated, the technology used within this work provides proof-of-concept evidence that targeting PSGL-1 in a spatially clustered manner improves protection against thrombosis. Ultimately, the goal of this work was to identify biological processes that could then be prophylactically prevented in high-risk patient populations. Building upon this, future work will explore small-molecule inhibitors of PSGL-1 using the clustering mechanics of the NPs that will allow for an effective and inexpensive treatment for chronic thrombotic diseases.

MATERIALS AND METHODS

Study design

This study tested the hypothesis that activated neutrophils are critical and targetable actors of arteriovenous thrombosis in a mouse model of APS. Further, we investigated transcriptional regulation of these processes by the transcription factor KLF2. We used cells isolated from patients with APS, mouse models of APS, and mice with myeloid-specific knockout of KLF2 to investigate the dynamics of neutrophil migration and adhesion and developed NPs targeting neutrophil adhesion as a treatment modality in these models using a ligation model of venous thrombosis and laser-induced injury model of arterial thrombosis. Sample sizes were determined on the basis of previous experimental experience and extensive review of the literature in the field. For experiments involving pharmacologic injection to mice, mice from each genotype were randomized into control or treatment groups such that littermates were dispersed into separate groups whenever possible. Investigators responsible for analyzing samples were blinded to the identity of the genotype, treatment, and disease state of the individuals from which the samples were derived. "*n*" refers to biological replicates. Molecular biology experiments were performed with at least three technical replicates. Surgical (thrombosis) experiments were performed using at least three trials.

Mice

All animal studies were performed in mice 8 to 12 weeks of age. All of the mice colonies were maintained in a clean animal facility, and all animal experimentation was approved by the Case Western Reserve University Institutional Animal Care and Use Committee. Myeloid-specific K2KO mice were generated by crossing the KLF2-floxed mice ($Klf2^{tm2Ling}$) (41) to the Lyz2Cre (the Jackson Laboratory). All wild-type mice are C57bl/6J (the Jackson Laboratory).

aPL treatment mouse model

Total IgG fractions from plasma obtained from patients with high titer aPLs and recurrent thrombotic events were provided by T. Ortel (Duke University). Mice aged 8 to 10 weeks received 20 μg of IgG intravenously obtained from patients with APS APA (Antiphospholipid Antibody Syndrome) or control IgG. Antibodies were administered at 24 and 6 hours before the arterial or venous thrombosis assays or before peripheral blood or bone marrow harvest.

Neutrophil and monocyte depletion

For neutrophil depletion studies, mice were injected with anti-Lymphocyte antigen 6 complex locus G6D (Ly6G) antibody (Bio X Cell, clone 1A8) at an initial concentration of 400 μg (injected retro-orbitally) 1 day before thrombosis assays and 100 μg (intraperitoneally) just before surgery. Greater than 80% depletion of peripheral neutrophils was achieved at 24 hours, when thrombosis assays were performed. For monocyte depletion, clodronate liposomes (Liposoma, C-005) were injected retro-orbitally 24 hours before surgery.

Two-photon imaging of the ear

Mice were anesthetized with isoflurane and then placed on their side. The ear was taped to the back of a chamber slide and covered with a drop of phosphate-buffered saline (PBS) so that the vessels could be visualized. Imaging was performed using a Leica SP5 equipped with a tunable Chameleon Ti/Sapphire laser-tuned to 800 nm. Thermal tissue damage was performed by turning the laser power to maximum for 5 s immediately before imaging. Rhodamine 6G (0.1%) (50 μl per mouse; Sigma-Aldrich) and anti-CD41 Alexa Fluor (AF) 647–labeled antibody (0.1 μg/g; BioLegend, MWReg30, catalog no. 133934) were injected intravenously 1 hour before imaging studies. High-resolution four-dimensional xyzt stacks were taken using a four channel nondescanned detector, and images were analyzed using Imaris software from Bitplane Inc.

Cortical actin quantification

Neutrophils were stained using the Cell Navigator F-actin staining kit (AAT Bioquest) and fixed in 4% paraformaldehyde. Neutrophils were stained without plating to avoid adhesion-based remodeling of actin. Cells were then coverslipped in mounting media, and confocal images were taken. Cortical actin abundance was quantified using averaged Z-stack measurements in ImageJ.

Luciferase reporter assay

Luciferase reporter assay plasmids driven by the TF promoter (−1.5 kb) (gift from N. Mackman, UNC, Chapel Hill) were transfected alone or were cotransfected with pcDNA3.1 or KLF2 plasmids in RAW264.7 cells using FuGENE (Promega) transfection reagent. Luciferase reporter activity was measured and normalized with the luciferase reporter assay systems as specified by the manufacturer's instructions, and the results are presented as relative luciferase activity over the control group.

Mouse carotid artery thrombosis assay

For the carotid artery thrombosis assay, mice 8 to 12 weeks of age were anesthetized by intraperitoneal injection with sodium pentobarbital and placed in the supine position on a dissecting microscope (Nikon SMZ-2T, Mager Scientific Inc.). A midline surgical incision was made to expose the right common carotid artery and a Doppler flow probe (model 0.5 VB, Transonic Systems) was placed under the vessel. The probe was connected to a flowmeter (Transonic model T106) and was interpreted with a computerized data acquisition program (Windaq, DATAQ Instruments). Rose Bengal [4,5,6,7-tetrachloro-3′,6-dihydroxy-2,4,5,7-tetraio-dospiro (isobenzofuran-1(3*H*),9[9*H*] xanthan)-3:1 dipotassium salt, Thermo Fisher Scientific] at 50 mg/kg in 0.9% saline] was then injected into the tail vein in a 0.12-ml volume (42). After injection into the tail vein, a green laser light (Melles Griot) at a wavelength of 540 nm was applied 6 cm from the carotid artery. Flow was monitored continuously from the onset of injury. The time to occlusion was determined only after the vessel remained closed with a cessation of blood flow for 20 min. For the aPL-mediated studies, mice were treated with 20 μg of total IgG purified from plasma samples obtained from patients with APS or controls (Thomas Ortel, Duke University) at the indicated times.

RNA sequencing and bioinformatics analyses

Peripheral blood neutrophils were isolated from LysM and K2KO mice ($n = 4$). RNA was isolated using the RNeasy Micro Kit (QIAGEN). RNA quantity and quality were checked using NanoDrop (Thermo Fisher Scientific) and Fragment Analyzer (Agilent), respectively. We used the NEBNext Ultra RNA Library Prep Kit for cells and the Directional RNA Library Prep Kit from Illumina to generate strand-specific libraries for endothelial cells. The analyses of the RNA sequencing datasets were performed through the genomic core of Case Western Reserve University. Before sequence alignment, trimgalore (version 0.4.3) with cutadapt package (version 1.12) was used for adaptor trimming and to improve data quality. For transcriptome alignment, we used STAR with GENCODE reference features. We then mapped sequencing reads to the mouse reference genome (mm10) using STAR aligner. DESeq2 packages were used for differential expression analysis. Variance-stabilizing transformation in DESeq2 was used for normalizing count data. Functional analysis of DEGs was performed using the Molecular Signature Database (Broad Institute).

Mouse IVC complete ligation venous thrombosis

The procedure was performed as previously described (43). Briefly, mice aged 8 to 12 weeks were anesthetized with isoflurane. Using sterile procedures, the abdominal cavity

was opened with a ventral midline incision. All IVC back branches, from renal veins to the iliac bifurcation, were cauterized and side branches are ligated. The IVC was separated from the aorta, just inferior to the renal veins and completely ligated with 7-0 prolene. The laparotomy site was then closed. The mice were allowed to recover and observed postoperatively for 2 hours before returning to their original housing units. IVC thrombi were harvested and weighed at 48 hours. At the time of euthanasia, blood was collected in sodium citrate for analysis and the IVC, with the thrombus, was harvested for thrombus weight.

Western blot analysis

Protein from bone marrow neutrophils was extracted using radio-immunoprecipitation assay (RIPA) buffer (Sigma-Aldrich, R0278) supplemented with proteinase and phosphatase inhibitor cocktails (Roche, 4693132001 and 4906845001). The protein concentration of the cell lysate was determined using Pierce bicinchoninic acid (BCA) protein assay kit (Thermo Fisher Scientific). The cell lysate were separated by 10% polyacrylamide gel electrophoresis gel and transferred to polyvinylidene difluoride membranes. Membranes were blocked for 1 hour with either 5% milk or 5% bovine serum albumin (BSA) in tris-buffered saline with Tween 20 (TBS-T). Primary antibodies were added overnight at a concentration of 1:500 to 1:2000 at 4° (see table S1 for details). After washing with TBS-T, horseradish peroxidase–conjugated secondary antibodies were added at a concentration of 1:5000 for 1 hour at room temperature. Membranes were then washed again with TBS-T and developed using Pierce SuperSignal West Dura chemiluminescence substrate kits and visualized using an imager from Azure Biosystems.

Isolation of bone marrow–derived neutrophils

Neutrophils were derived from the bone marrow of mice as previously described (44). Briefly, under sterile conditions, bone marrow cells from bilateral femur and tibia of each mice (age 8 to 12 weeks) were flushed and collected. Red cell lysis was performed using hypotonic sodium chloride at 0.2% for 20 s, followed by 1.6% sodium chloride. Neutrophils were then purified from the bone marrow cells using a Histopaque-based density gradient centrifugation. Cells were routinely assessed to be greater than 95% pure by Wright-Giemsa stain and have greater than 95% viability as measured by trypan blue staining. Bone marrow from each mouse (two femurs and two tibias) yielded 6 million to 12 million neutrophils. Neutrophil TF activity was assessed in cellular lysates using the TF activity assay kit (Abcam, ab108906).

Adoptive neutrophil transfer studies

Neutrophils obtained from the bone marrow of stated mice were transfused into each mouse for either carotid artery thrombosis or IVC venous thrombosis assays. Briefly, bone marrow–derived neutrophils isolated as described above were washed twice in PBS, followed by resuspension in PBS to a density of 5×10^7 cells/ml. A total of 5×10^6 cells in a volume of 100 μl were injected retro-orbitally in each mouse for each thrombosis assay. All neutrophil transfusions were completed within 6 hours of bone marrow harvest to ensure neutrophil viability.

Neutrophil flow studies

The neutrophils were flown through IBIDI microfluidic channels coated or uncoated with P-selectin (50 μg/ml; R&D Systems, 737-PS), ICAM-1 (R&D Systems, 796-IC), or VCAM-1 (R&D Systems, 643-VM) protein. For some studies, neutrophils were preincubated with anti–PSGL-1 (Bio X Cell, BE0186) or control isotype antibody (Bio X Cell, BE0088) or with coated NPs as indicated before flow studies. The flow rate was set at 14 μl/min or 1 dyn·s/cm^2. This is normal shear in large veins. Analysis was performed with ICY image analysis software running on m5.large instance at Amazon Web Services. Statistics and graphing were done in Aable NG.

Boyden chamber transwell migration assay

Cell migration was evaluated using Transwell plates (24-well format, 8-μm pore size; BD Falcon). Neutrophils were resuspended at 1×10^6 cells/ml in medium supplemented with 1% fetal bovine serum, and 5×10^5 cells were seeded in the upper chamber. Recombinant CXCL12 or CCL21 (R&D Systems) in medium containing 1% fetal bovine serum was used as chemoattractants in the lower compartment. The chambers were incubated overnight at 37°C. Cells on the upper surface of the membrane were removed using a cotton-wool swab. Migrated cells on the lower surface were stained with crystal violet, and the number of migrated cells was counted in five medium power fields (magnification, ×100). Results are expressed as the mean number of net migrated cells ± SD. Each experiment was done in triplicate.

*f*MLP-induced neutrophil recruitment into peritoneal cavity

Indicated mice received an intraperitoneal injection of *f*MLP (50 μg in 100 μl of saline) to stimulate neutrophil-rich peritoneal exudates. At the indicated times, animals were euthanized by isoflurane inhalation, and peritoneal cavities were washed with 4 ml of RPMI 1640 with 10% fetal bovine serum containing 3 mM EDTA. The recovered cells were counted using a Neubauer chamber, and the percentage of neutrophils in the cellular exudate was determined by examination of a Wright-Giemsa–stained smear.

In vitro generation of NETs

Bone marrow–derived neutrophils were resuspended in RPMI 1640 with Hepes and allowed to adhere at 37°C in 5% CO_2 to glass-bottom plates (previously coated with poly-L-lysine) for 20 min before stimulation with LPS (10 μg/ml) from *Klebsiella pneumoniae* (Sigma-Aldrich). After 2 hours, cells were fixed in 2% (v/v) paraformaldehyde. Cells were then stained for citrullinated histone 3 as described below.

Immunostaining and fluorescence microscopy

Fixed cells or vessels were washed with PBS and permeabilized (0.1% Triton X-100 and 0.1% sodium citrate) for 10 min at 4°C. Samples were blocked with 3% (w/v) BSA for 90 min at 37°C, rinsed, and then incubated overnight at 4°C or for 1 hour at 37°C in antibody dilution buffer containing 0.3% BSA, 0.1% Tween 20, and relevant antibodies (rabbit anti-histone H3 (citrulline 2, 8, and 17) (0.3 μg/ml; Abcam, ab5103), rat anti–PSGL-1 (1:1000; BD Biosciences). After several washes, samples were incubated for

2 hours at room temperature in antibody dilution buffer containing AF 488–conjugated secondary antibody (1.5 μg/ml) in 0.3% BSA in PBS. DNA was counterstained with Hoechst 33342 (1 μg/ml), and slides were coverslipped with Fluoromount gel (Electron Microscopy Sciences). Fluorescent images were acquired using an Axiovert 200 widefield fluorescence microscope (Zeiss) in conjunction with an Axiocam MRm monochromatic charge-coupled device camera (Zeiss) and analyzed with Zeiss AxioVision software. All channels were acquired in grayscale and pseudo-colored using Zeiss AxioVision or ImageJ software (National Institutes of Health). Exposure times are identical between LysM-Cre and K2KO tissue or neutrophils. Images were analyzed using ImageJ.

Real-time quantitative polymerase chain reaction

Total RNA was extracted from bone marrow–derived neutrophils using TRIzol reagent (Invitrogen). Total RNA was extracted, treated with deoxyribonuclease I (Life Technologies, 18068015), and purified using the RNeasy MinElute Cleanup Kit (QIAGEN, 74204). Two micrograms of total RNA was reverse-transcribed to complementary DNA using the iScript Reverse Transcription Kit (Bio-Rad, 170-8841). Real-time polymerase chain reaction (PCR) was performed using the Universal SYBR Green method on the ViiA 7 Real-Time PCR System (Applied Biosystems). Relative expression was calculated using the $\Delta\Delta C_t$ method with normalization to *Gapdh*. Primer sequences are shown in table S2.

PSGL-1 NP synthesis, purification, and characterization

FluoSpheres carboxylate-modified microspheres [NP template (NT)], such as Thermo Fisher Scientific, F8786, at a concentration of 2% solids in water, were pH-adjusted with 1 M Hepes buffer (pH 8) to a stable pH of 7.0. Next, the solution of 1-ethyl-3-(3-dimethylaminopropyl)carbodiimide (EDAC; Thermo Fisher Scientific, E2247) at 10 mg/ml in water was added to the pH-adjusted NT at 0.1 mg of EDAC per 1 mg of NT. The solution was bath-sonicated on ice for 5 min, and a second portion of EDAC was added to the solution at the same ratio of NT to EDAC. The mixture was pH-adjusted again, maintaining the pH at 7.0, and bath-sonicated on ice for 10 min. The activated NT was separated from unreacted EDAC by ultracentrifugation (100,000*g* for 20 min at 4°C) for 0.02- and 0.1-μm NT or high-speed centrifugation (31,000*g* for 10 min at 4°C) for 0.2-, 0.5-, 1-, and 2-μm NT. The supernatant was removed using vacuum suction and the pellet was reconstituted by bath sonication in 100 mM Hepes-buffered saline buffer (HBS; pH 7.0, 150 mM NaCl) at 1% NT solids. Next, InVivoMAb anti-mouse PSGL-1 (Bio X Cell, BE0186) antibody was added to the activated NT at 1 mg of mAb per 1 mg of NT. The solution was bath-sonicated on ice for 10 min and then incubated at room temperature for 1 hour with end-over rotation. The anti–PSGL-1–coated NPs were then separated from the solution using ultracentrifugation or high-speed centrifugation as described above. The pellet was reconstituted by bath sonication in HBS and additionally purified by passing through a Zeba desalting column (40-kDa molecular weight cutoff; Thermo Fisher Scientific, 87766) according to the manufacturer's instructions. To synthesize the IgG-coated NPs, BioLegend 400602 isotope rat IgG1κ was used instead of anti-mouse PSGL-1 in the same manner. NPs produced from 0.02-, 0.1-, and 0.2-μm NTs were filter-sterilized using 0.45-μm Polyethersulfone (PES) membranes. Large-size nano/microparticles (0.5 to 2 μm) were prepared in aseptic conditions and were used without additional filtration.

The NPs were characterized using dynamic light scattering using the Zetasizer Nano ZS instrument (Malvern Instruments). NPs were diluted in water at 0.01%, and standard latex operating procedures were used. At least 15 measurement cycles were used for each sample. To determine antibody concentration in NP preparations, protein and polystyrene were first precipitated from an aliquot of NPs by addition of 10 volumes of acetone and incubated at −80°C for at least 1 hour. Next, the precipitate was separated using centrifugation (31,000*g* for 10 min at 4°C), and the supernatant was removed. The protein was extracted from this pellet by sonication in RIPA buffer [50 mM tris-HCl (pH 7.4), 150 mM NaCl, 1% NP-40, 0.5% sodium deoxycholate, and 0.1% SDS) plus 50 mM dithiothreitol. The extract was cleared using centrifugation (31,000*g* for 10 min at 4°C) and the protein concentration was determined using the BCA assay (Thermo Fisher Scientific, 23250).

NP size optimization was performed using a fluorescence-based method. A total of 4×10^5 bone marrow–derived neutrophils from LysM and K2KO mice were treated with anti–PSGL-1 NPs of various sizes (0.02 to 1.0 μm). Fluorescent readouts were recorded after incubation at 37°C for 30 min (565-nm excitation, 605-nm emission). Cells were counterstained with Hoechst, and fluorescent values were recorded again. Serial dilutions of Hoechst-stained neutrophils were used to determine the number of cells per well, and serial dilutions of NPs were used to determine the concentrations of NPs present in each well. Fitting data to a standard curve provided the amount of NPs bound per cell.

Tail bleeding assay

Tail bleeding times were measured by transecting the tails of anesthetized mice [sodium pentobarbital (50 mg/kg)] 5 mm from the tip. The tail was placed in 10 ml of saline at 37°C. The time to cessation of bleeding for 20 s was determined with a stopwatch.

Statistical analysis

Raw, individual-level data are presented in data file S1. Statistical analysis comparing two groups was performed by Mann-Whitney *U* test or unpaired two-tailed *t* test with Welch's correction to account for unequal SDs, as appropriate. Data were also tested for normality using the Shapiro-Wilk test and for equality of variances using the Bartlett's test. In cases where normality and equality of variances were not rejected at the significance level of 0.05, the group means were compared using pairwise *t* test with Holm correction or analysis of variance (ANOVA) with Tukey's post hoc test. All statistical analysis was performed using GraphPad Prism software version 8 or the latest version of R. Statistical significance was defined as $P < 0.05$ unless stated otherwise.

Supplementary Material

Refer to Web version on PubMed Central for supplementary material.

Acknowledgments:

We thank T. Ortel for providing patient-derived aPL for our studies. Similarly, we thank D. Kirchhofer at Genentech for providing the rat anti-mouse 1H1 TF-neutralizing antibody. We also thank J. Diaz for the instruction on the venous ligation model and support and M.-Q. Du for providing the KLF2 mutant expression plasmids.

Funding:

This work was supported by NIH grants R01DK111478, R35HL135789, and R01HL086548 (to M.K.J.); R01HL142647 (to L.N.); T32GM007250 and F30HL139014 (to D.R.S.); and R01HL130516 and R01HL155450 (to A. Maiseyeu). This work was also supported by the American Heart Association-Allen Frontiers Award (to M.K.J.) and the Leducq Foundation Transatlantic Network of Excellence (to M.K.J.).

REFERENCES AND NOTES

1. Secomb TW, Hemodynamics. Compr. Physiol 6, 975–1003 (2016). [PubMed: 27065172]
2. Aird WC, Phenotypic heterogeneity of the endothelium. Circ. Res 100, 174–190 (2007). [PubMed: 17272819]
3. Pfeiler S, Stark K, Massberg S, Engelmann B, Propagation of thrombosis by neutrophils and extracellular nucleosome networks. Haematologica 102, 206–213 (2017). [PubMed: 27927771]
4. von Brühl ML, Stark K, Steinhart A, Chandraratne S, Konrad I, Lorenz M, Khandoga A, Tirniceriu A, Coletti R, Köllnberger M, Byrne RA, Laitinen I, Walch A, Brill A, Pfeiler S, Manukyan D, Braun S, Lange P, Riegger J, Ware J, Eckart A, Haidari S, Rudelius M, Schulz C, Echtler K, Brinkmann V, Schwaiger M, Preissner KT, Wagner DD, Mackman N, Engelmann B, Massberg S, Monocytes, neutrophils, and platelets cooperate to initiate and propagate venous thrombosis in mice in vivo. J. Exp. Med 209, 819–835 (2012). [PubMed: 22451716]
5. Kapoor S, Opneja A, Nayak L, The role of neutrophils in thrombosis. Thromb. Res 170, 87–96 (2018). [PubMed: 30138777]
6. Mahabeleshwar GH, Kawanami D, Sharma N, Takami Y, Zhou G, Shi H, Nayak L, Jeyaraj D, Grealy R, White M, Manus RM, Ryan T, Leahy P, Lin Z, Haldar SM, Atkins GB, Wong HR, Lingrel JB, Jain MK, The myeloid transcription factor KLF2 regulates the host response to polymicrobial infection and endotoxic shock. Immunity 34, 715–728 (2011). [PubMed: 21565532]
7. Nayak L, Goduni L, Takami Y, Sharma N, Kapil P, Jain MK, Mahabeleshwar GH, Kruppel-like factor 2 is a transcriptional regulator of chronic and acute inflammation. Am. J. Pathol 182, 1696–1704 (2013). [PubMed: 23499374]
8. Nayak L, Shi H, Atkins GB, Lin Z, Schmaier AH, Jain MK, The thromboprotective effect of bortezomib is dependent on the transcription factor Kruppel-like factor 2 (KLF2). Blood 123, 3828–3831 (2014). [PubMed: 24771858]
9. Vorobjeva NV, Chernyak BV, NETosis: Molecular mechanisms, role in physiology and pathology. Biochem. Mosc 85, 1178–1190 (2020).
10. Reinhardt C, von Brühl M-L, Manukyan D, Grahl L, Lorenz M, Altmann B, Dlugai S, Hess S, Konrad I, Orschiedt L, Mackman N, Ruddock L, Massberg S, Engelmann B, Protein disulfide isomerase acts as an injury response signal that enhances fibrin generation via tissue factor activation. J. Clin. Invest 118, 1110–1122 (2008). [PubMed: 18274674]
11. Clipson A, Wang M, de Leval L, Ashton-Key M, Wotherspoon A, Vassiliou G, Bolli N, Grove C, Moody S, Escudero-Ibarz L, Gundem G, Brugger K, Xue X, Mi E, Bench A, Scott M, Liu H, Follows G, Robles EF, Martinez-Climent JA, Oscier D, Watkins AJ, du M-Q, KLF2 mutation is the most frequent somatic change in splenic marginal zone lymphoma and identifies a subset with distinct genotype. Leukemia 29, 1177–1185 (2015). [PubMed: 25428260]
12. Knight JS, Meng H, Coit P, Yalavarthi S, Sule G, Gandhi AA, Grenn RC, Mazza LF, Ali RA, Renauer P, Wren JD, Bockenstedt PL, Wang H, Eitzman DT, Sawalha AH, Activated signature of antiphospholipid syndrome neutrophils reveals potential therapeutic target. JCI Insight 2, e93897 (2017). [PubMed: 28931754]
13. von Andrian UH, Hasslen SR, Nelson RD, Erlandsen SL, Butcher EC, A central role for microvillous receptor presentation in leukocyte adhesion under flow. Cell 82, 989–999 (1995). [PubMed: 7553859]
14. Weiner OD, Servant G, Welch MD, Mitchison TJ, Sedat JW, Bourne HR, Spatial control of actin polymerization during neutrophil chemotaxis. Nat. Cell Biol 1, 75–81 (1999). [PubMed: 10559877]
15. Hind LE, Vincent WJ, Huttenlocher A, Leading from the back: The role of the uropod in neutrophil polarization and migration. Dev. Cell 38, 161–169 (2016). [PubMed: 27459068]

16. Bruehl RE, Moore KL, Lorant DE, Borregaard N, Zimmerman GA, McEver RR, Bainton DF, Leukocyte activation induces surface redistribution of P-selectin glycoprotein ligand-1. J. Leukoc. Biol 61, 489–499 (1997). [PubMed: 9103236]
17. Alonso-Lebrero JL, Serrador JM, Domínguez-Jiménez C, Barreiro O, Luque A, del Pozo MA, Snapp K, Kansas G, Schwartz-Albiez R, Furthmayr H, Lozano F, Sánchez-Madrid F, Polarization and interaction of adhesion molecules P-selectin glycoprotein ligand 1 and intercellular adhesion molecule 3 with moesin and ezrin in myeloid cells. Blood 95, 2413–2419 (2000). [PubMed: 10733515]
18. Miner JJ, Xia L, Yago T, Kappelmayer J, Liu Z, Klopocki AG, Shao B, McDaniel JM, Setiadi H, Schmidtke DW, McEver RP, Separable requirements for cytoplasmic domain of PSGL-1 in leukocyte rolling and signaling under flow. Blood 112, 2035–2045 (2008). [PubMed: 18550846]
19. Tinoco R, Otero DC, Takahashi AA, Bradley LM, PSGL-1: A new player in the immune checkpoint landscape. Trends Immunol. 38, 323–335 (2017). [PubMed: 28262471]
20. Wong DJ, Park DD, Park SS, Haller CA, Chen J, Dai E, Liu L, Mandhapati AR, Eradi P, Dhakal B, Wever WJ, Hanes M, Sun L, Cummings RD, Chaikof EL, A PSGL-1 glycomimetic reduces thrombus burden without affecting hemostasis. Blood 138, 1182–1193 (2021). [PubMed: 33945603]
21. Patel MS, Miranda-Nieves D, Chen J, Haller CA, Chaikof EL, Targeting P-selectin glycoprotein ligand-1/P-selectin interactions as a novel therapy for metabolic syndrome. Transl. Res 183, 1–13 (2017). [PubMed: 28034759]
22. Yago T, Liu Z, Ahamed J, McEver RP, Cooperative PSGL-1 and CXCR2 signaling in neutrophils promotes deep vein thrombosis in mice. Blood 132, 1426–1437 (2018). [PubMed: 30068506]
23. Bagalkot V, Badgeley MA, Kampfrath T, Deiuliis JA, Rajagopalan S, Maiseyeu A, Hybrid nanoparticles improve targeting to inflammatory macrophages through phagocytic signals. J. Control. Release 217, 243–255 (2015). [PubMed: 26386437]
24. Sweet DR, Vasudevan NT, Fan L, Booth CE, Keerthy KS, Liao X, Vinayachandran V, Takami Y, Tugal D, Sharma N, Chan ER, Zhang L, Qing Y, Gerson SL, Fu C, Wynshaw-Boris A, Sangwung P, Nayak L, Holvoet P, Matoba K, Lu Y, Zhou G, Jain MK, Myeloid Krüppel-like factor 2 is a critical regulator of metabolic inflammation. Nat. Commun 11, 5872 (2020). [PubMed: 33208733]
25. Pengo V, Biasiolo A, Pegoraro C, Cucchini U, Noventa F, Iliceto S, Antibody profiles for the diagnosis of antiphospholipid syndrome. Thromb. Haemost 93, 1147–1152 (2005). [PubMed: 15968401]
26. Borghi MO, Raschi E, Grossi C, Chighizola CB, Meroni PL, Toll-like receptor 4 and β2 glycoprotein I interaction on endothelial cells. Lupus 23, 1302–1304 (2014). [PubMed: 25228733]
27. Laplante P, Amireault P, Subang R, Dieudé M, Levine JS, Rauch J, Interaction of β2-glycoprotein I with lipopolysaccharide leads to Toll-like receptor 4 (TLR4)-dependent activation of macrophages. J. Biol. Chem 286, 42494–42503 (2011). [PubMed: 21965665]
28. Xie H, Sheng L, Zhou H, Yan J, The role of TLR4 in pathophysiology of antiphospholipid syndrome-associated thrombosis and pregnancy morbidity. Br. J. Haematol 164, 165–176 (2014). [PubMed: 24180619]
29. Das H, Kumar A, Lin Z, Patino WD, Hwang PM, Feinberg MW, Majumder PK, Jain MK, Kruppel-like factor 2 (KLF2) regulates proinflammatory activation of monocytes. Proc. Natl. Acad. Sci. U.S.A 103, 6653–6658 (2006). [PubMed: 16617118]
30. Bisso PW, Gaglione S, Guimarães PPG, Mitchell MJ, Langer R, Nanomaterial interactions with human neutrophils. ACS Biomater Sci. Eng 4, 4255–4265 (2018). [PubMed: 31497639]
31. Chu D, Dong X, Shi X, Zhang C, Wang Z, Neutrophil-based drug delivery systems. Adv. Mater 30, e1706245 (2018). [PubMed: 29577477]
32. Da Costa Martins P, García-Vallejo J-J, van Thienen JV, Fernandez-Borja M, van Gils JM, Beckers C, Horrevoets AJ, Hordijk PL, Zwaginga J-J, P-Selectin glycoprotein ligand-1 is expressed on endothelial cells and mediates monocyte adhesion to activated endothelium. Arterioscler. Thromb. Vasc. Biol 27, 1023–1029 (2007). [PubMed: 17322099]
33. An G, Wang H, Tang R, Yago T, McDaniel JM, McGee S, Huo Y, Xia L, P-selectin glycoprotein ligand-1 is highly expressed on Ly-6C^{hi} monocytes and a major determinant for Ly-6C^{hi} monocyte

recruitment to sites of atherosclerosis in mice. Circulation 117, 3227–3237 (2008). [PubMed: 18519846]

34. Frenette PS, Denis CV, Weiss L, Jurk K, Subbarao S, Kehrel B, Hartwig JH, Vestweber D, Wagner DD, P-selectin glycoprotein ligand 1 (PSGL-1) is expressed on platelets and can mediate platelet-endothelial interactions in vivo. J. Exp. Med 191, 1413–1422 (2000). [PubMed: 10770806]
35. Hirata T, Merrill-Skoloff G, Aab M, Yang J, Furie BC, Furie B, P-Selectin glycoprotein ligand 1 (PSGL-1) is a physiological ligand for E-selectin in mediating T helper 1 lymphocyte migration. J. Exp. Med 192, 1669–1676 (2000). [PubMed: 11104809]
36. Hoffmann MAG, Bar-On Y, Yang Z, Gristick HB, Gnanapragasam PNP, Vielmetter J, Nussenzweig MC, Bjorkman PJ, Nanoparticles presenting clusters of CD4 expose a universal vulnerability of HIV-1 by mimicking target cells. Proc. Natl. Acad. Sci. U.S.A 117, 18719–18728 (2020). [PubMed: 32690692]
37. Baroni G, Banzato A, Bison E, Denas G, Zoppellaro G, Pengo V, The role of platelets in antiphospholipid syndrome. Platelets 28, 762–766 (2017). [PubMed: 28267395]
38. Velásquez M, Rojas M, Abrahams VM, Escudero C, Cadavid ÁP, Mechanisms of endothelial dysfunction in antiphospholipid syndrome: Association with clinical manifestations. Front. Physiol 9, 1840 (2018). [PubMed: 30627104]
39. Simonin L, Pasquier E, Leroyer C, Cornec D, Lemerle J, Bendaoud B, Hillion S, Pers J-O, Couturaud F, Renaudineau Y, Lymphocyte disturbances in primary antiphospholipid syndrome and application to venous thromboembolism follow-up. Clin Rev Allergy Immunol 53, 14–27 (2017). [PubMed: 27342459]
40. Mulder WJM, Ochando J, Joosten LAB, Fayad ZA, Netea MG, Therapeutic targeting of trained immunity. Nat. Rev. Drug Discov 18, 553–566 (2019). [PubMed: 30967658]
41. Weinreich MA, Takada K, Skon C, Reiner SL, Jameson SC, Hogquist KA, KLF2 transcription-factor deficiency in T cells results in unrestrained cytokine production and upregulation of bystander chemokine receptors. Immunity 31, 122–130 (2009). [PubMed: 19592277]
42. Eitzman DT, Westrick RJ, Nabel EG, Ginsburg D, Plasminogen activator inhibitor-1 and vitronectin promote vascular thrombosis in mice. Blood 95, 577–580 (2000). [PubMed: 10627465]
43. Wrobleski SK, Farris DM, Diaz JA, Myers DD Jr., Wakefield TW, Mouse complete stasis model of inferior vena cava thrombosis. J. Vis. Exp, 2738 (2011).
44. Swamydas M, Luo Y, Dorf ME, Lionakis MS, Isolation of mouse neutrophils. Curr. Protoc. Immunol 110, 3.20.1–3.20.15 (2015).

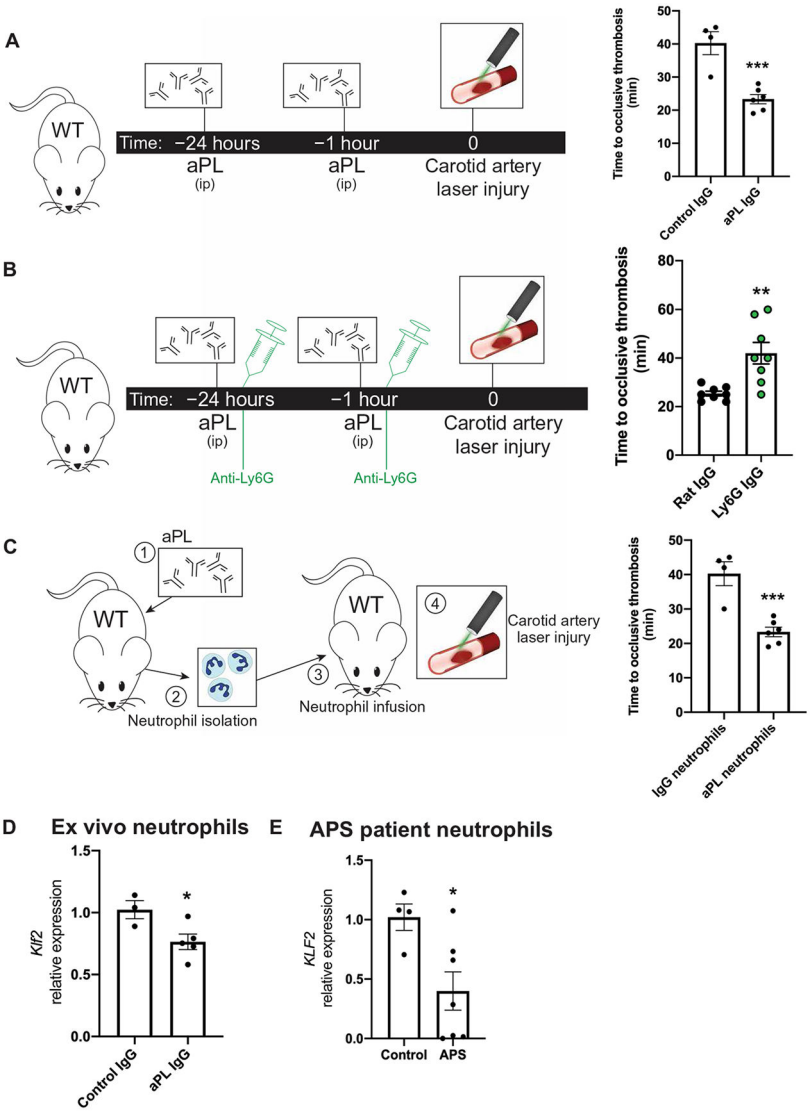

Fig. 1. Activated neutrophils drive arterial and venous thrombosis.

(**A**) In the murine antiphospholipid antibody (aPL)–injected model, mice were injected intraperitoneally (ip) with either aPL isolated from patients with APS (n = 6 mice) or IgG isolated from healthy controls (n = 4 mice) at 24 hours and 1 hour before a carotid artery laser-induced injury model of thrombosis. Time to occlusive thrombus development was measured. (**B**) Neutrophil depletion in aPL-treated mice using anti-Ly6G antibody (n = 8 mice) or control IgG (n = 8 mice) was followed by carotid artery injury to measure dependency on neutrophils in arterial thrombus formation. Time to occlusive thrombosis development was measured. All mice received aPLs. (**C**) Neutrophils were harvested from IgG- or aPL-treated wild-type (WT) mice and transferred into untreated WT mice (n = 4 IgG-treated neutrophil recipients; n = 6 aPL-treated neutrophil recipients) before carotid artery injury. (**D**) *Klf2* expression was measured in neutrophils harvested from IgG-injected (n = 3) or aPL-injected (n = 5) WT mice. (**E**) *KLF2* expression was measured in neutrophils

harvested from humans with APS ($n = 7$) or healthy controls ($n = 4$). *$P < 0.05$, **$P < 0.01$, and ***$P < 0.001$ by unpaired, two-tailed Student's t test.

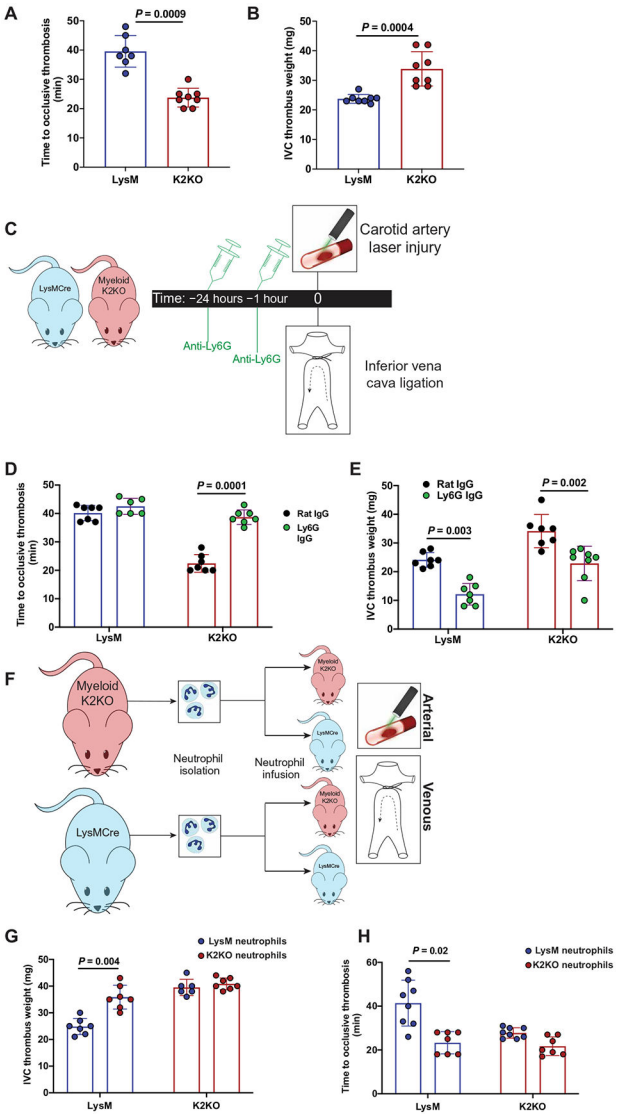

Fig. 2. Neutrophil activation through loss of KLF2 worsens arterial and venous thrombosis.

(**A**) Time to occlusive thrombosis was measured in the carotid artery injury model comparing LysM ($n = 7$) and K2KO ($n = 8$) mice. (**B**) IVC thrombus weight measured after IVC ligation comparing LysM and K2KO mice. $n = 8$ mice. (**C**) The timeline shows the experimental model of neutrophil depletion studies in K2KO mice. (**D** and **E**) Neutrophils were depleted with anti-Ly6G antibody or control antibody in LysM ($n = 6$ to 7) and K2KO ($n = 6$ to 8) mice before (D) arterial or (E) venous thrombosis induction. (**F**) The timeline depicts adoptive transfer experiments wherein neutrophils were isolated from healthy LysM or K2KO mice and infused into LysM/K2KO mice before arterial or venous thrombosis. (**G** and **H**) Infusion of LysM (CRE) or K2KO (KO) neutrophils into respective genotypes ($n =$ 6 to 8 per group) was followed by initiation of (G) arterial and (H) venous thrombosis. Data were analyzed using an unpaired, two-tailed Student's *t* test.

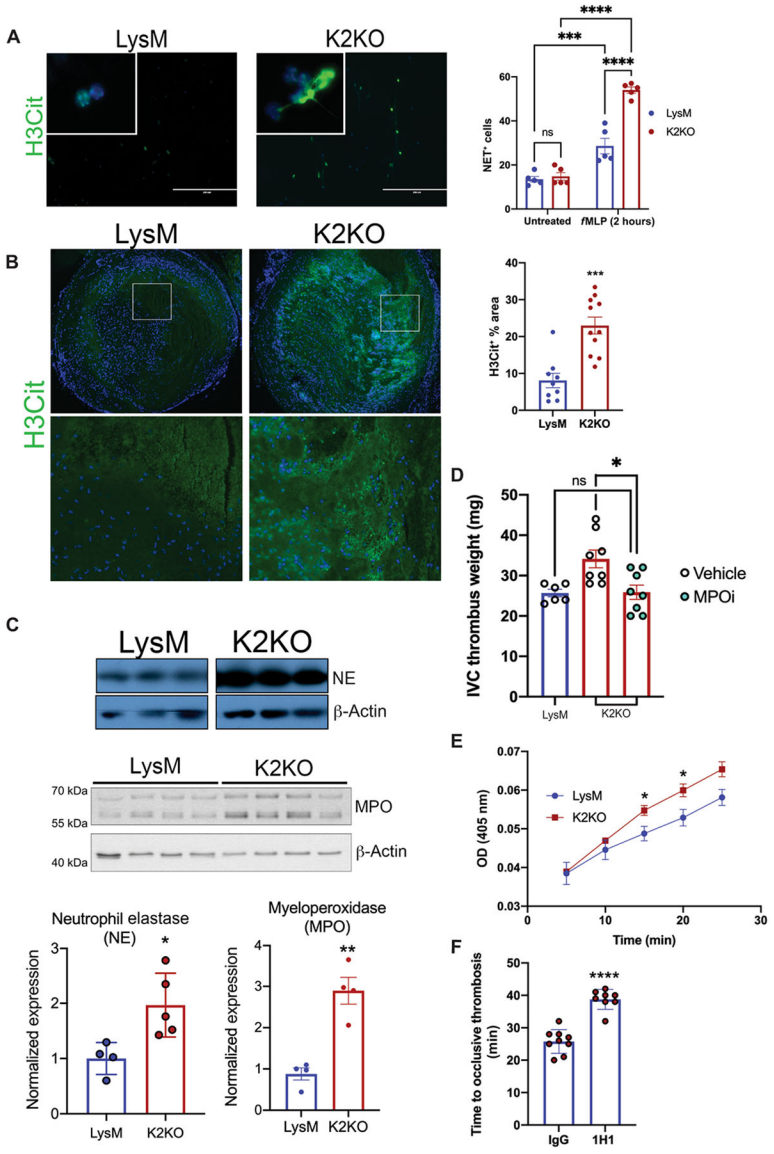

Fig. 3. Loss of KLF2 permits prothrombotic neutrophil functions.

(**A**) Neutrophil extracellular trap (NET) staining with citrullinated histone 3 (H3Cit) is shown for *N*-formyl-Met-Leu-Phe (*f*MLP)-stimulated LysM or K2KO neutrophils in vitro ($n = 5$). (**B**) H3Cit NET staining within harvested clots after IVC ligation was quantified (LysM, $n = 9$; K2KO, $n = 11$). Quantification represents the percentage of clot area that is $H3Cit^+$. (**C**) Western blot of cell lysate from unstimulated LysM and K2KO neutrophils measuring neutrophil elastase (NE) and myeloperoxidase (MPO) abundance is shown. Quantification is normalized to β-actin. (**D**) LysM ($n = 6$) and K2KO [vehicle, $n = 8$; MPO inhibitor (MPOi), $n = 8$] mice received an MPOi before the IVC thrombosis model in mice; thrombus weight was measured. (**E**) A colorimetric tissue factor (TF) activity assay was used to measure conversion of factor X to Xa over time in LysM and K2KO neutrophils ($n = 3$ to 5). OD, optical density. (**F**) The effect of TF neutralization before carotid artery thrombosis was measured. K2KO neutrophils were incubated with either

control or TF-neutralizing antibody (1H1) before infusion into LysM mice (IgG, $n = 9$; 1H1, $n = 8$). *$P < 0.05$, **$P < 0.01$, ***$P < 0.001$, and ****$P < 0.0001$ by unpaired, two-tailed Student's t test.

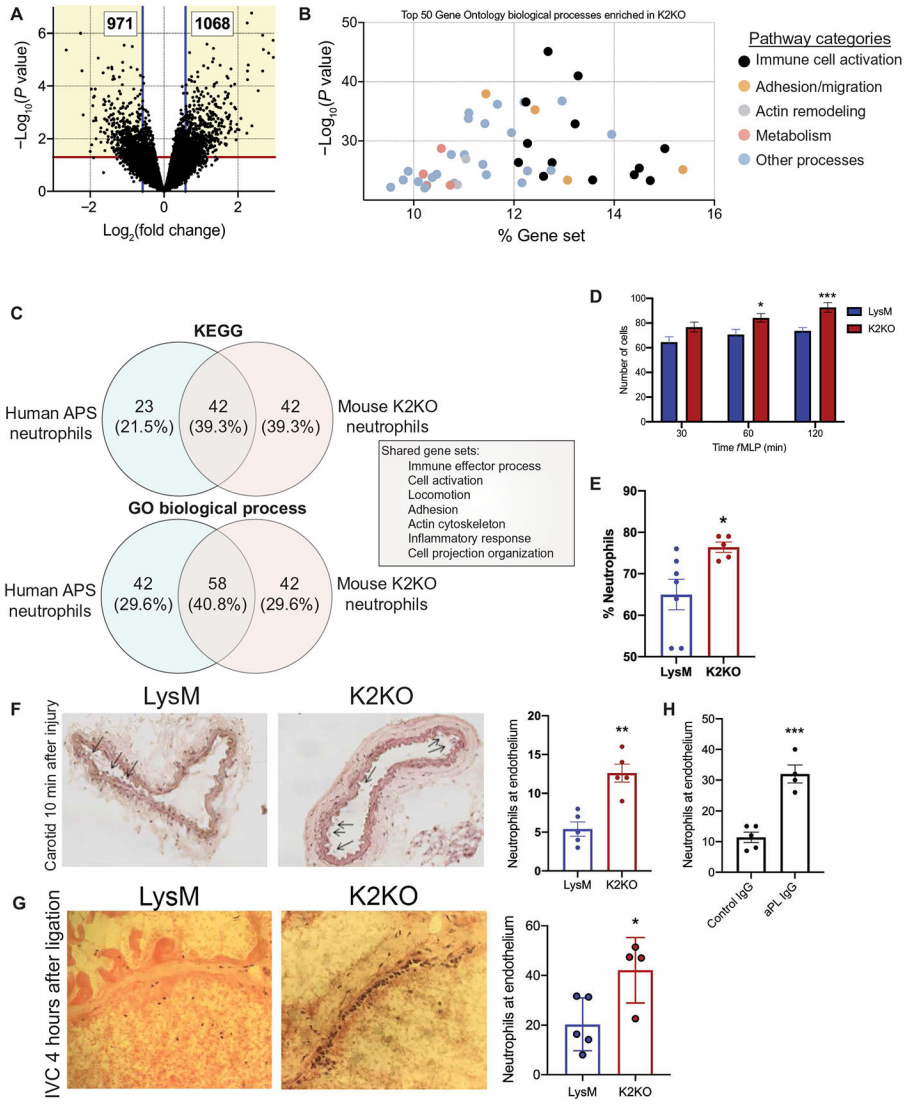

Fig. 4. Activated neutrophils are transcriptionally primed for prothrombotic adhesion and migration.

(**A**) The volcano plot from RNA sequencing of peripheral blood neutrophils demonstrates more than 2000 differentially expressed genes between K2KO and LysM cells. (**B**) Gene Ontology (GO) biological process analysis of differentially expressed genes from K2KO neutrophil RNA sequencing is shown. % Gene set represents the proportion of the entire process that is affected by loss of KLF2. (**C**) The overlap of enriched pathways between K2KO neutrophils and neutrophils from humans with APS is shown. (**D**) Results of a transwell migration experiment using *N*-formyl-Met-Leu-Phe (*f*MLP) as chemoattractant for LysM and K2KO neutrophils are shown ($n = 10$ to 12). (**E**) Peritoneal lavage after *f*MLP intraperitoneal injection was used to quantify neutrophil migration in LysM ($n = 7$) and K2KO ($n = 5$) mice. (**F** and **G**) Ly6G-stained neutrophils were quantified along vessel walls early after (F) carotid artery injury (10 min) and (G) IVC ligation (4 hours) are shown for LysM and K2KO mice ($n = 4$ to 5). (**H**) Neutrophils were quantified along vessel walls early

after carotid artery injury in IgG-injected ($n = 5$) or aPL-injected ($n = 4$) WT mice. *$P <$ 0.05, **$P < 0.01$, and ***$P < 0.001$ by unpaired, two-tailed Student's t test.

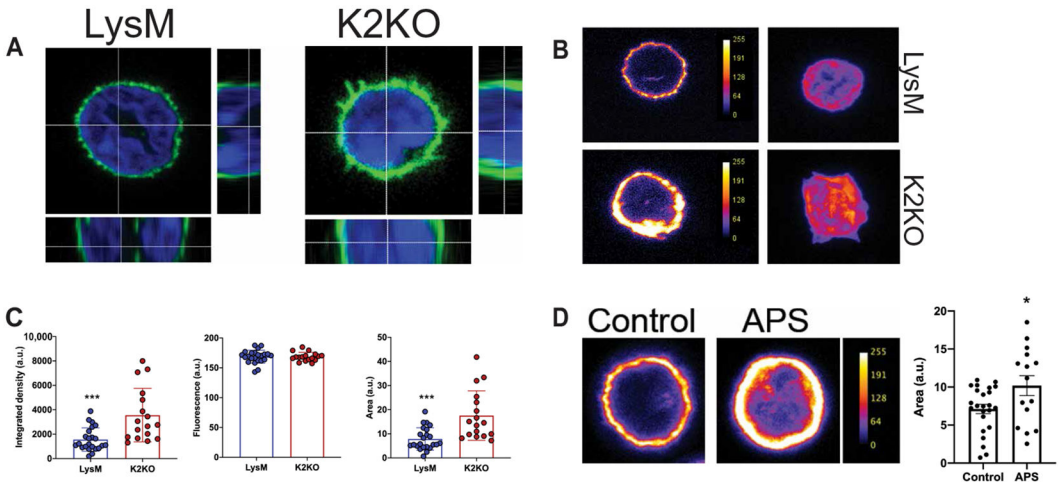

Fig. 5. Neutrophil activation is associated with cortical actin remodeling in K2KO and APS neutrophils.

(**A**) Confocal microscopy of F-actin–stained neutrophils demonstrates cortical actin alignment in untreated LysM and K2KO neutrophils. (**B**) Fluorescent intensity of cortical F-actin expression in untreated LysM and K2KO neutrophils is shown. (**C**) Quantification of actin area, fluorescence intensity, and integrated density from confocal images is shown. LysM, $n = 23$ cells from three mice; K2KO, $n = 19$ cells from three mice. (**D**) Cortical actin staining is shown for neutrophils isolated from either healthy controls ($n = 25$ cells from three donors) or patients with APS ($n = 15$ cells from three donors). Scales in (B) and (D) indicate cortical actin fluorescence intensity. a.u., arbitrary units. *$P < 0.05$ and ***$P < 0.001$ by unpaired, two-tailed Student's t test.

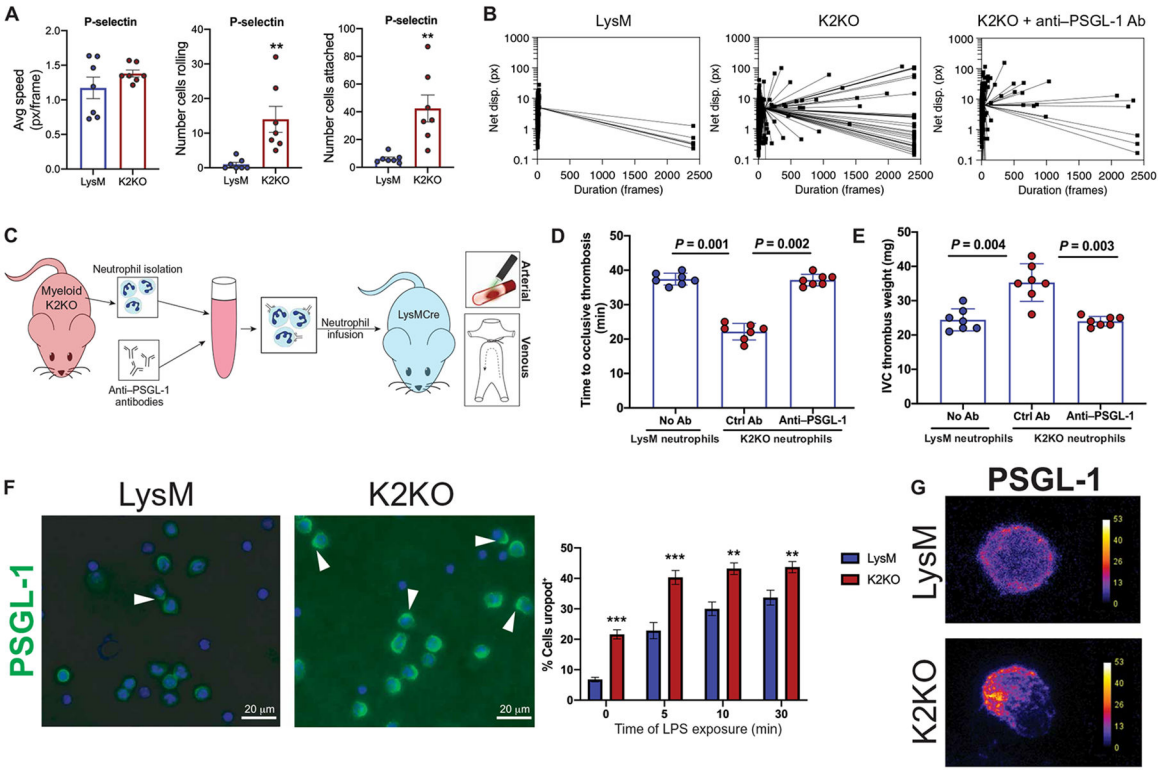

Fig. 6. PSGL-1 clustering facilitates prothrombotic K2KO neutrophil adhesion.

(**A**) Measurement of flowing speed, extent of rolling, and adhesion is shown for LysM and K2KO neutrophils in microfluidic channels coated with P-selectin. Avg, average; px, pixels. (**B**) Dot plots depict the duration of time that each cell remained in the field of view. Neutrophils from LysM mice, K2KO mice, and K2KO mice pretreated ex vivo with anti–PSGL-1 antibody (Ab) were compared. (**C**) An experimental outline is shown where neutrophils were isolated from K2KO mice, incubated with either control or anti–PSGL-1 antibodies, and infused into LysM mice before the arterial or venous thrombosis models. (**D** and **E**) The effect of anti–PSGL-1 antibody-treated K2KO neutrophils on (D) arterial and (E) venous thrombosis is shown. Blue dots depict neutrophils from LysM mice, and red dots depict neutrophils from K2KO mice. All cells were infused into LysM mice ($n = 7$ per group). (**F**) PSGL-1 staining in LPS-treated LysM and K2KO neutrophils is shown with quantification of uropod$^+$ cells ($n = 5$ to 6). Uropods are indicated with an arrowhead. Scale bars, 20 μm. (**G**) Confocal images depict uropod formation, as demonstrated by polarized PSGL-1 clustering. Scales indicate PSGL-1 fluorescence intensity. $^{**}P < 0.01$ and $^{***}P < 0.001$ by unpaired, two-tailed Student's t test.

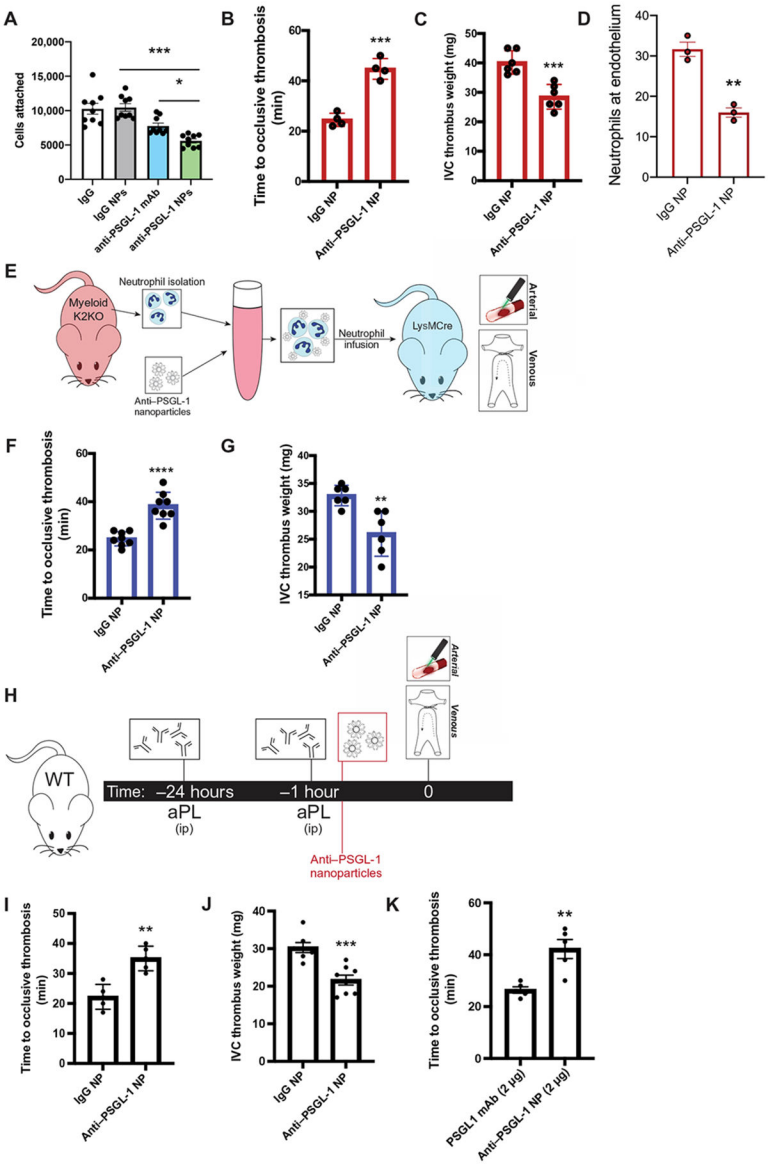

Fig. 7. Targeting PSGL-1 clustering in activated neutrophils with decorated nanoparticles protects against arterial and venous thrombosis.

(**A**) Cell attachment quantification from in vitro microfluidic assay is shown. K2KO neutrophils were preincubated with control IgG, anti–PSGL-1 antibody, control IgG NP, or anti–PSGL-1 NP before flowing through chambers ($n = 9$ trials). (**B** and **C**) The extent of thrombosis in K2KO mice treated with IgG or anti–PSGL-1–coated NP was compared for both (B) arterial and (C) venous models ($n = 4$ arterial and $n = 6$ venous). (**D**) Quantification of neutrophils along vessel walls early after carotid artery injury is shown for K2KO mice treated with either IgG ($n = 3$) or anti–PSGL-1 ($n = 3$) NPs. (**E**) The experimental design for adoptive neutrophil transfer is shown. Neutrophils from K2KO mice were incubated with IgG or anti–PSGL-1 NPs and transferred into LysM mice before thrombosis. (**F** and **G**) K2KO neutrophils preincubated with either IgG or anti–PSGL-1 NPs were infused into LysM mice before (F) carotid artery injury or (G) IVC ligation ($n = 6$ to 8). (**H**) An

experimental timeline is shown depicting treatment of aPL-injected WT mice with either IgG or anti–PSGL-1 NPs before thrombosis induction. (**I** and **J**) The effect of anti–PSGL-1 NP treatment against aPL-induced (I) arterial and (J) venous thrombosis was measured (n = 5 to 8). (**K**) Lower doses of anti–PSGL-1 antibody were compared in an aPL-injected carotid artery injury model (n = 5). Anti–PSGL-1 was administered either alone or in NP formulation at concentrations of 2 μg. *P < 0.05, **P < 0.01, ***P < 0.001, and ****P < 0.0001 by unpaired, two-tailed Student's t test.